

Biological Impact of Ozone Depletion at the End-Permian: A modeling study

Brian C. Thomas and Jacob M. Oberle

Washburn University, Department of Physics and Astronomy

1700 SW College Ave., Topeka, KS USA 66621

brian.thomas@washburn.edu

Abstract:

The end-Permian mass extinction is the most severe known from the fossil record. The most likely cause is massive volcanic activity associated with the formation of the Permo-Triassic Siberian flood basalts. A proposed mechanism for extinction due to this volcanic activity is depletion of stratospheric ozone, leading to increased penetration of biologically damaging Solar ultraviolet-B (UVB) radiation to Earth's surface. Previous work has modeled the atmospheric chemistry effects of volcanic emission at the end-Permian. Here we use those results as input for detailed radiative transfer simulations to investigate changes in surface-level Solar irradiance in the ultraviolet-B, ultraviolet-A and photosynthetically available (visible light) wave bands. We then evaluate the potential biological effects using biological weighting functions. In addition to changes in ozone column density we also include gaseous sulfur dioxide (SO₂) and sulfate aerosols. Ours is the first such study to include these factors and we find they have a significant impact on transmission of Solar radiation through the atmosphere. Inclusion of SO₂ and aerosols greatly reduces the transmission of radiation across the ultraviolet

and visible wavelengths, with subsequent reduction in biological impacts by UVB. We conclude that claims of a UVB mechanism for this extinction are likely overstated.

Introduction

The end-Permian mass extinction is the most severe extinction known with at least 80% of marine, and 70% of terrestrial species disappearing from the fossil record¹⁻⁴. The leading hypothesis for the cause of the “great dying” is volcanic activity associated with the formation of the Permo-Triassic Siberian flood basalts⁵⁻⁸. The mechanisms of extinction include climate change^{6,9}, ocean acidification⁶, and ozone depletion^{5-7,10,11}. Depletion of stratospheric ozone (O_3) leads to increased solar ultraviolet-B (UVB, 280-315 nm) irradiance at Earth’s surface, which is known to have significant negative impacts on aquatic (both marine¹² and freshwater¹³) and terrestrial organisms^{11,14-17}. Evidence of UVB-induced damage at the end-Permian comes from malformed spores and pollens^{7,11,14,18} and recent experimental work has directly connected UVB exposure to malformation and sterilization of modern conifers¹¹; a massive die-off of coniferous vegetation is associated with the extinction event¹⁹.

Changes in atmospheric chemistry, including depletion of O_3 have been studied using a 2D chemistry-transport model¹⁰ as well as a 3D Earth system model⁵. Both studies found significant O_3 depletion, but the level of depletion depends on details of the volcanic activity such as duration, type of eruption, and amounts and types of particular gasses emitted. In the most severe cases modeled, column density depletion of O_3 ranges from 60-85%, depending on latitude^{5,10}, while less severe cases yield depletion of 20-40%.

The gasses HCl, CH₃Cl, and CH₄ are particularly important in the ozone depletion process. The amount of these gasses emitted depends on the local geological conditions at the time and the nature of the eruptions. The ability to affect O₃ depends on whether these gasses can reach the stratosphere. Evidence indicates that the Siberian eruptions were likely extensive²⁰ and explosive¹⁰ enough to inject significant amounts of these gasses into the stratosphere. In addition, the tropospheric lifetime of CH₃Cl is long enough (greater than one year) for significant amounts to be transported into the stratosphere, even if it is not directly injected there by the eruptions. Strong evidence exists to support very large emission of volatiles, including the important O₃-depleting species, during the Siberian eruptions^{7,8,20}. It has been shown that the high extinction rate during the period lines up best with sill intrusion through a volatile-rich basin²⁰. Therefore, the combined geological evidence appears to make the most severe O₃ depletion cases^{5,10} realistic.

Atmospheric modeling data

In this work we use results of the most recent and comprehensive modeling of atmospheric conditions at the end-Permian⁵. This modeling considered a variety of possible volcanic conditions, resulting in a range of O₃ depletion cases. We acquired data files for a case (“A2” in that work) that is slightly less severe than the most extreme model result, making our results somewhat conservative (from the perspective of O₃

depletion), given the possible range of impacts that are supported by the available geological evidence.

While O₃ is the most important atmospheric constituent controlling transmission of UVB (280-315 nm), volcanically produced SO₂ gas and sulfate (H₂SO₄) aerosols are also important. Broadly speaking, increased SO₂ column density and aerosol optical depth (AOD) lead to reduced transmission of UVB. A recent study²¹ used the Tropospheric Ultraviolet and Visible (TUV) 1D radiative transfer model²²

(<https://www2.acom.ucar.edu/modeling/tropospheric-ultraviolet-and-visible-tuv-radiation-model>), to examine the effect on surface-level UVB irradiance by changes in these constituents. In this study, we use the methodology described in that work, applied to the specific conditions likely to have been in place during the Siberian Traps volcanic episode. While an earlier study¹⁰ examined the effect of O₃ depletion alone at the end-Permian, ours is the first such study to include variations in SO₂ and sulfate aerosols, both of which are radiatively important and major atmospheric constituents during volcanic episodes.

Radiative Transfer Modeling

We use version 5.0 of the TUV model. TUV allows the user to modify a variety of parameter values, including date, time, location (latitude and longitude), altitude, and column density and vertical profile of O₃ and SO₂. Several aerosol optical parameters

can be modified: total aerosol optical depth (AOD), single scattering albedo (SSA), Angstrom coefficient (α), a wavelength-independent scattering asymmetry factor (g), and vertical profiles. The default aerosol profile in TUV is for modern continental conditions, with AOD = 0.235, SSA = 0.99, $\alpha = 1.0$, and $g = 0.61$.

We performed several simulations in order to evaluate the effects of varying different constituents. As a control, we use annual average O₃ column density values, as a function of latitude and longitude, from the control run in the modeling study by Black et al.⁵ (hereafter “Black14”) with globally uniform SO₂ column density of 0.05 DU and the default TUV aerosol parameters. The other simulation cases are presented in Table 1, where “Black14 A2” refers to (depleted) O₃ column density values from Siberian Traps volcanism case A2 in the Black14 study. In all cases the SO₂ and aerosol values are globally uniform. While the volcanic emission is not global, a recent study²³ found volcanic events that inject SO₂ into the stratosphere result in a roughly global distribution of gaseous SO₂ and sulfate aerosols, so our simplifying assumption is reasonable. In addition, our analysis will focus on broad comparisons rather than detailed geographic distribution of impacts.

We have chosen two “volcanic” aerosol cases. In both cases SSA = 0.99, $\alpha = 2.0$, $g = 0.74$, and the altitude profile is a combined “flood” and “stratospheric” case; these parameter and profile choices are described in more detail in our previous work²¹. The combined low- and high-altitude profile is chosen as the best fit to the Siberian Traps eruption event^{10,24}. In aerosol case 1 we use AOD = 0.5 and in case 2 AOD = 2.0;

these values are likely lower and upper limits for the period of active volcanism²⁵. The other aerosol parameters are not varied since their effect on UVB transmission is relatively small, compared to that of AOD.²¹ For SO₂ we take a value of 10.0 DU during the volcanic episode.²⁶

The data we acquired from Black14 gives an annual average of O₃ column density as a function of latitude and longitude. In order to incorporate effects of seasonal variation on solar zenith angle we ran TUV at 1 day each month for 1 year, at local noon, at each longitude-latitude point. We then averaged over the 12 time points to give a single annual average value at each spatial point.

Results

We are interested in how changes in O₃ column density modeled for the end-Permian volcanic conditions affect surface-level Solar irradiance and subsequent biological impacts. In order to evaluate the impact of the reduced O₃, we have examined ratios of various values computed using the O₃ column density in the Black14 A2 volcanic case versus the Black14 control case.

Figure 1 shows the ratio of O₃ column density in the Black14 A2 volcanic case versus the Black14 control case. The depletion of O₃ is significant across the globe, with the largest change in the North polar region. In general, O₃ depletion is greatest in the

polar regions due to factors including atmospheric transport and polar stratospheric clouds, and in this case the volcanic emissions are larger in the Northern hemisphere, leading to higher depletion in the North.

Figure 2 shows the ratio of computed surface-level UVB irradiance in the O₃-depleted (volcanic) case versus control. As expected, the increase in UVB irradiance tracks the decrease in O₃ column density. The increase is significant globally, with very large increases Northward of about 45° latitude, and Southward of about 55° latitude.

Longitudinal variation is present in the O₃ variation due to geographical and volcanic emission variation in the climate model simulation. Since we are interested in more general impacts, the rest of our results and discussion will focus on zonally or globally averaged values.

Figure 3 shows the zonally averaged ratio of UVB irradiance for each of our volcanic cases versus control. The case labels refer to those listed in Table 1. For instance, the “O₃ + SO₂ + aer 2” case includes the volcanic case O₃ column density, our prescribed SO₂ column density, and our prescribed “aerosol 2” values. In every case, the same depleted (and control) O₃ column density distribution is used.

Notice in this plot that the latitude distribution of the ratios are all similar (as we would expect, since the O₃ column density distribution is the same for all cases), but the magnitude of the ratio is quite different between cases. Notably, the two cases that include our high optical depth “aerosol 2” settings show *reduced* irradiance compared to

the control case, in the equatorial regions, where O₃ depletion is less severe. The high aerosol optical depth leads to much lower UVB irradiance compared to cases with lower optical depth.

In order to simplify comparisons between cases, Figures 4-12 show globally averaged ratios for several irradiance bands and biological weighting functions (BWFs). Note in Figure 4 that the high optical depth “aer2” cases show much lower ratios (as also seen in Figure 3). With SO₂ included with the high aerosol optical depth, the globally averaged ratio is 0.995, meaning the UVB irradiance is actually slightly *lower* than in the control case despite O₃ depletion.

Figure 5 shows results for UVA (315-400 nm), a biologically important waveband. In every case, except O₃ depletion only, there is less UVA irradiance compared to control, with less than half in the SO₂ plus high aerosol optical depth case. Similarly, Figure 6 shows results for photosynthetically available radiation (PAR, 400-700 nm), with lower irradiance compared to control in every case except O₃ depletion only.

Figure 7 shows results for erythema-weighted irradiance ratios. Erythema is a commonly used proxy for biological damage, but refers to skin damage and is therefore only relevant to relatively complex organisms. Erythema tracks closely with UVB, and the ratios here show a similar pattern, high for the O₃ depletion case, but much reduced under the addition of SO₂ and high optical depth aerosols.

Figures 8-10, show results for photosynthesis inhibition in phytoplankton. The largest increase is seen in Figure 8, using a BWF for inhibition of carbon fixation in a natural Antarctic phytoplankton community²⁷. Figures 9 and 10 show results using BWFs for inhibition of photosynthesis in the phytoplankton species *Phaeo-dactylum* (“phaeo”) and *Prorocentrum micans* (“proro”), respectively²⁸. Again we note that inclusion of high optical depth aerosols leads to *reduced* inhibition of photosynthesis. However, with reduction in PAR (seen above) these results do not necessarily indicate an *increase* in productivity. Fully evaluating the effect on phytoplankton primary productivity will require more extensive modeling that incorporates a weighting function spanning the full UVB-UVA-PAR range^{29,30}.

A recent study¹¹ (hereafter “Benca18”) has attempted to detect evidence of UVB exposure of gymnosperms at the end-Permian, using observations of malformed fossilized pollen grains compared to pollen grains of similar modern-day species that were exposed to specific levels of UVB irradiance under controlled conditions. That study used biologically weighted UVB exposure, calculated using a weighting function for land plants³¹ (referred to here as “Caldwell71”). Figure 11 shows our results using this same BWF, again looking at globally averaged ratios of weighted irradiance in our various cases compared to the control. Notice that the vertical scale on this plot is larger than on the previous ones. This particular BWF is very sensitive to changes in UVB, much more so than another plant BWF³² (referred to here as “Flint_Caldwell03”) shown in Figure 12. Figure 13 shows the zonally averaged ratio for the Caldwell71 BWF; the pattern in latitude tracks that of the UVB ratio, but the range of values is much

larger. However, as with other comparisons, the effect is greatly reduced with the addition of high optical depth aerosols and SO₂.

For their study of trees, Benca18 used daily integrated Caldwell71-weighted UVB flux. Their outdoor tree population (located in Berkeley, CA) was exposed to 7.2 kJ m⁻² day⁻¹. For Permian exposure, Benca18 used the only existing estimates of Permian plant damage-weighted UV levels, taken from a 2D atmospheric chemistry modeling study¹⁰ (hereafter, "Beerling07"). In that work, modeled background (no volcanic perturbation) exposure was found to be 10-20 kJ m⁻² day⁻¹, and O₃ depleted values ranged 40-100 kJ m⁻² day⁻¹.

In order to make direct comparisons between our results and the Benca18 and Beerling07 values, we ran TUV hourly, one day per month, for one year, using zonally averaged O₃ column density values. The hourly Caldwell71-weighted irradiance results were then daily-integrated. Our Permian control case gives maximum flux values of around 8 kJ m⁻² day⁻¹, which is similar to the Benca18 modern day outdoor exposure. However, our value here is smaller than the Permian control values from Beerling07.

For our Permian O₃-depleted only case, we found maximum flux values of around 20 kJ m⁻² day⁻¹, which is significantly smaller than the Beerling07 maximum value. For our Permian O₃-depleted with SO₂ and high optical depth aerosol case, we found maximum flux values of around 6 kJ m⁻² day⁻¹, smaller even than the control case.

Overall then, even considering only O₃ depletion, we find lower Caldwell71-weighted flux values compared to Beerling07, and much smaller values when including SO₂ and high optical depth aerosols.

Discussion and Conclusions

Our study represents the most detailed examination to date of surface-level exposure to Solar UVB under probable end-Permian conditions. We have used a state-of-the-art radiative transfer model with best-estimate conditions for this time period. Broadly, we find that there is a large increase in UVB exposure, and subsequent biological impacts, in the O₃ depleted case – as much as an order of magnitude higher in North polar areas where depletion is greatest.

However, we also find that inclusion of SO₂ gas and sulfate aerosols has a major effect, greatly reducing exposure, in some cases even below what would be expected in a normal O₃ column density case. This is a significant result because it indicates that UVB exposure may not be as much of a contributor to the end-Permian extinction event as has been previously claimed.

We also find that previous plant damage weighted flux values given in the literature for this time period may be over estimated. The cause for the difference between our results and those of Beerling07 is not obvious and difficult to track down since few details are given in that work as to how flux values were arrived at. However, the most

likely cause is simplification or neglect of processes such as scattering by that work, where are accurately included in our modeling. A study³³ comparing simplified radiative transfer methods to results from the TUV model found that the simplified method overestimated UVB irradiance by a factor of about 2, depending on specific parameter values chosen.

Our results indicate that observations of malformed fossilized pollen¹¹ may not actually track increased UVB exposure, but may instead show exposure to heightened surface-level SO₂ concentration¹⁰, which also certainly accompanies major volcanic activity.

There are many potential sources of uncertainty in this work, most importantly a lack of knowledge about the SO₂ and aerosol conditions during this period. Our results likely bracket the maximum and minimum values that are realistic for the end-Permian volcanic episodes.

Finally, we note that ours is the first study to examine changes in surface level irradiance in the UVA and PAR bands for the end-Permian, and we find reduced levels in all cases except the O₃ depleted only case. The biological implications of this are not obvious and will require more extensive modeling that includes effects of the full UVB-UVA-PAR wavelength range.

Acknowledgements:

The authors thank Benjamin Black for providing data and assistance in processing that data into a format usable for this study.

Analysis and plotting was done using the NCAR Command Language (Version 6.5.0) [Software]. (2018). Boulder, Colorado: UCAR/NCAR/CISL/TDD.

<http://dx.doi.org/10.5065/D6WD3XH5>

References

1. Erwin, D. H. The Permo–Triassic extinction. *Nature* **367**, 231–236 (1994).
2. Knoll, A. H., Bambach, R. K., Payne, J. L., Pruss, S. & Fischer, W. W. Paleophysiology and end-Permian mass extinction. *Earth Planet. Sci. Lett.* **256**, 295–313 (2007).
3. Stanley, S. M. Estimates of the magnitudes of major marine mass extinctions in earth history. *Proc. Natl. Acad. Sci.* **113**, E6325–E6334 (2016).
4. Benton, M. J. & Twitchett, R. J. How to kill (almost) all life: The end-Permian extinction event. *Trends Ecol. Evol.* **18**, 358–365 (2003).
5. Black, B. A., Lamarque, J.-F., Shields, C. A., Elkins-Tanton, L. T. & Kiehl, J. T. Acid rain and ozone depletion from pulsed Siberian Traps magmatism. *Geology* **42**, 67–70 (2014).
6. Bond, D. P. G. & Grasby, S. E. On the causes of mass extinctions. *Palaeogeogr. Palaeoclimatol. Palaeoecol.* **478**, 3–29 (2017).
7. Broadley, M. W., Barry, P. H., Ballentine, C. J., Taylor, L. A. & Burgess, R. End-Permian extinction amplified by plume-induced release of recycled lithospheric volatiles. *Nat. Geosci.* **11**, 682–687 (2018).
8. Burgess, S. D., Muirhead, J. D. & Bowring, S. A. Initial pulse of Siberian Traps sills as the trigger of the end-Permian mass extinction. *Nat. Commun.* **8**, 164 (2017).
9. Kiehl, J. T. & Shields, C. A. Climate simulation of the latest Permian: Implications for mass extinction. *Geology* **33**, 757 (2005).

10. Beerling, D. J., Harfoot, M., Lomax, B. & Pyle, J. A. The stability of the stratospheric ozone layer during the end-Permian eruption of the Siberian Traps. *Philos. Trans. R. Soc. A Math. Phys. Eng. Sci.* **365**, 1843–1866 (2007).
11. Benca, J. P., Duijnste, I. A. P. & Looy, C. V. UV-B–induced forest sterility: Implications of ozone shield failure in Earth’s largest extinction. *Sci. Adv.* **4**, e1700618 (2018).
12. Llabrés, M. *et al.* Impact of elevated UVB radiation on marine biota : a meta-analysis. 131–144 (2013). doi:10.1111/j.1466-8238.2012.00784.x
13. Peng, S., Liao, H., Zhou, T. & Peng, S. Effects of UVB radiation on freshwater biota : a meta-analysis. 500–510 (2017). doi:10.1111/geb.12552
14. Visscher, H. *et al.* Environmental mutagenesis during the end-Permian ecological crisis. *Proc. Natl. Acad. Sci.* **101**, 12952–12956 (2004).
15. Bornman, J. F. *et al.* Solar ultraviolet radiation and ozone depletion-driven climate change: effects on terrestrial ecosystems. *Photochem. Photobiol. Sci.* **14**, 88–107 (2015).
16. Caldwell, M. M. *et al.* Effects of increased solar ultraviolet radiation on terrestrial ecosystems. **46**, 40–52 (1998).
17. Ballaré, C. L., Caldwell, M. M., Flint, S. D., Robinson, S. A. & Bornman, J. F. Effects of solar ultraviolet radiation on terrestrial ecosystems. Patterns, mechanisms, and interactions with climate change. *Photochem. Photobiol. Sci.* **10**, 226–241 (2011).
18. Foster, C. B. & Afonin, S. A. Abnormal pollen grains: an outcome of deteriorating atmospheric conditions around the Permian-Triassic boundary. *J. Geol. Soc.*

- London*. **162**, 653–659 (2005).
19. Looy, C. V *et al.* The delayed resurgence of equatorial forests after the permian-triassic ecologic crisis. *Proc. Natl. Acad. Sci. U. S. A.* **96**, 13857–62 (1999).
 20. Burgess, S. D. & Bowring, S. A. High-precision geochronology confirms voluminous magmatism before, during, and after Earth's most severe extinction. *Sci. Adv.* **1**, 1–14 (2015).
 21. Thomas, B. C., Goracke, B. D. & Dalton, S. M. Atmospheric constituents and surface-level UVB: Implications for a paleoaltimetry proxy and attempts to reconstruct UV exposure during volcanic episodes. *Earth Planet. Sci. Lett.* (2016). doi:10.1016/j.epsl.2016.08.014
 22. Madronich, S. & Flocke, S. Theoretical Estimation of Biologically Effective UV Radiation at the Earth's Surface. in *Solar Ultraviolet Radiation* 23–48 (Springer Berlin Heidelberg, 1997). doi:10.1007/978-3-662-03375-3_3
 23. Zambri, B., Robock, A., Mills, M. J. & Schmidt, A. Modeling the 1783–1784 Laki Eruption in Iceland: 1. Aerosol Evolution and Global Stratospheric Circulation Impacts. *J. Geophys. Res. Atmos.* **124**, 6750–6769 (2019).
 24. Campbell, I. H., Czamanske, G. K., Fedorenko, V. A., Hill, R. I. & Stepanov, V. Synchronism of the Siberian traps and the Permian-Triassic boundary. *Science* (80-.). **258**, 1760–1763 (1992).
 25. Schmidt, A. *et al.* Selective environmental stress from sulphur emitted by continental flood basalt eruptions. *Nat. Geosci.* **9**, 77–82 (2016).
 26. Schmidt, A. *et al.* Satellite detection, long-range transport, and air quality impacts of volcanic sulfur dioxide from the 2014-2015 flood lava eruption at Bárðarbunga

- (Iceland). *J. Geophys. Res. Atmos.* **120**, 9739–9757 (2015).
27. Boucher, N. *et al.* Icecolors '93: Biological weighting function for the ultraviolet inhibition of carbon fixation in a natural antarctic phytoplankton community. *Antarct. J. Rev.* 272–275 (1994).
 28. Cullen, J. J., Neale, P. J. & Lesser, M. P. Biological Weighting Function for the Inhibition of Phytoplankton Photosynthesis by Ultraviolet Radiation. *Science* (80-.). **258**, 646–650 (1992).
 29. Neale, P. J. & Thomas, B. C. Solar irradiance changes and phytoplankton productivity in earth's ocean following astrophysical ionizing radiation events. *Astrobiology* **16**, (2016).
 30. Neale, P. J. & Thomas, B. C. Inhibition by ultraviolet and photosynthetically available radiation lowers model estimates of depth-integrated picophytoplankton photosynthesis: global predictions for *Prochlorococcus* and *Synechococcus*. *Glob. Chang. Biol.* **23**, 293–306 (2017).
 31. Caldwell, M. M. SOLAR UV IRRADIATION AND THE GROWTH AND DEVELOPMENT OF HIGHER PLANTS. in *Photophysiology* 131–177 (Elsevier, 1971). doi:10.1016/b978-0-12-282606-1.50010-6
 32. Flint, S. D. & Caldwell, M. M. A biological spectral weighting function for ozone depletion research with higher plants. *Physiol. Plant.* **117**, 137–144 (2003).
 33. Thomas, B. C., Neale, P. J. & Snyder, B. R. Solar Irradiance Changes and Photobiological Effects at Earth's Surface Following Astrophysical Ionizing Radiation Events. *Astrobiology* **15**, 207–220 (2015).

Table 1: Atmospheric constituent cases. “volc” refers to our volcanic aerosol and SO₂ profiles; “aer 1” and “aer 2” refer to our two aerosol cases.

Case	O ₃	SO ₂ (DU)	SO ₂ profile	AOD	SSA	α	g	aerosol profile
Control	Black14 Control	0.05	TUV default	0.235	0.99	1.0	0.61	TUV default
O ₃ only	Black14 A2	0.05	TUV default	0.235	0.99	1.0	0.61	TUV default
O ₃ + aer 1	Black14 A2	0.05	TUV default	0.5	0.99	2.0	0.74	volc
O ₃ + aer 2	Black14 A2	0.05	TUV default	2.0	0.99	2.0	0.74	volc
O ₃ + SO ₂	Black14 A2	10.0	volc	0.235	0.99	1.0	0.61	TUV default
O ₃ + SO ₂ + aer 1	Black14 A2	10.0	volc	0.5	0.99	2.0	0.74	volc
O ₃ + SO ₂ + aer 2	Black14 A2	10.0	volc	2.0	0.99	2.0	0.74	volc

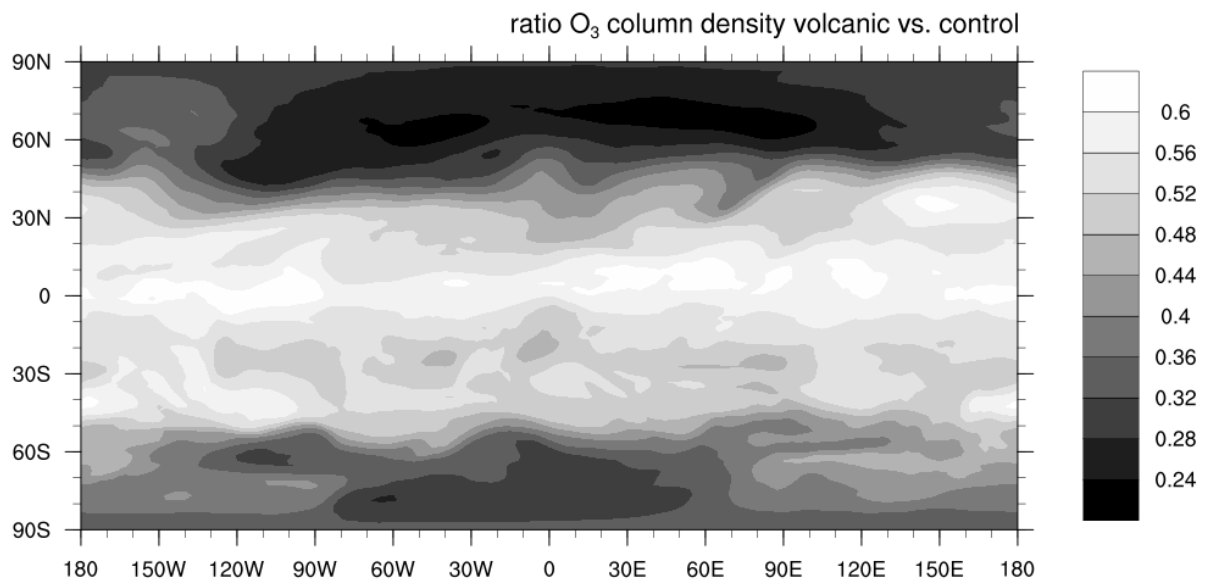


Figure 1 – Ratio of O₃ column density in the Black14 A2 volcanic case versus the Black14 control case.

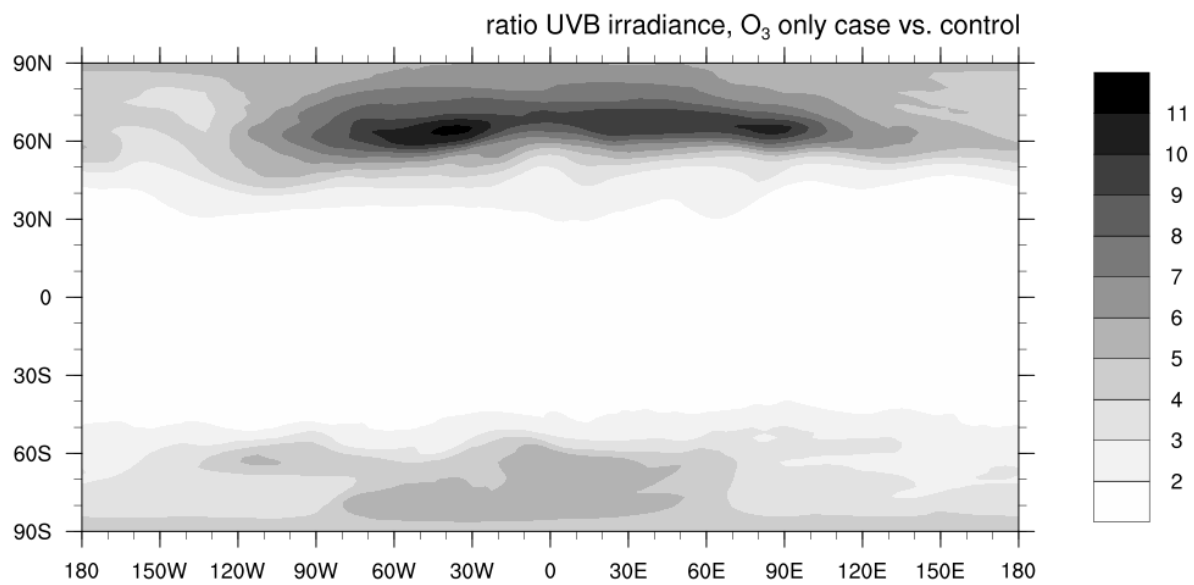


Figure 2 – Ratio of computed surface-level UVB irradiance in the O₃-depleted (volcanic) case versus control.

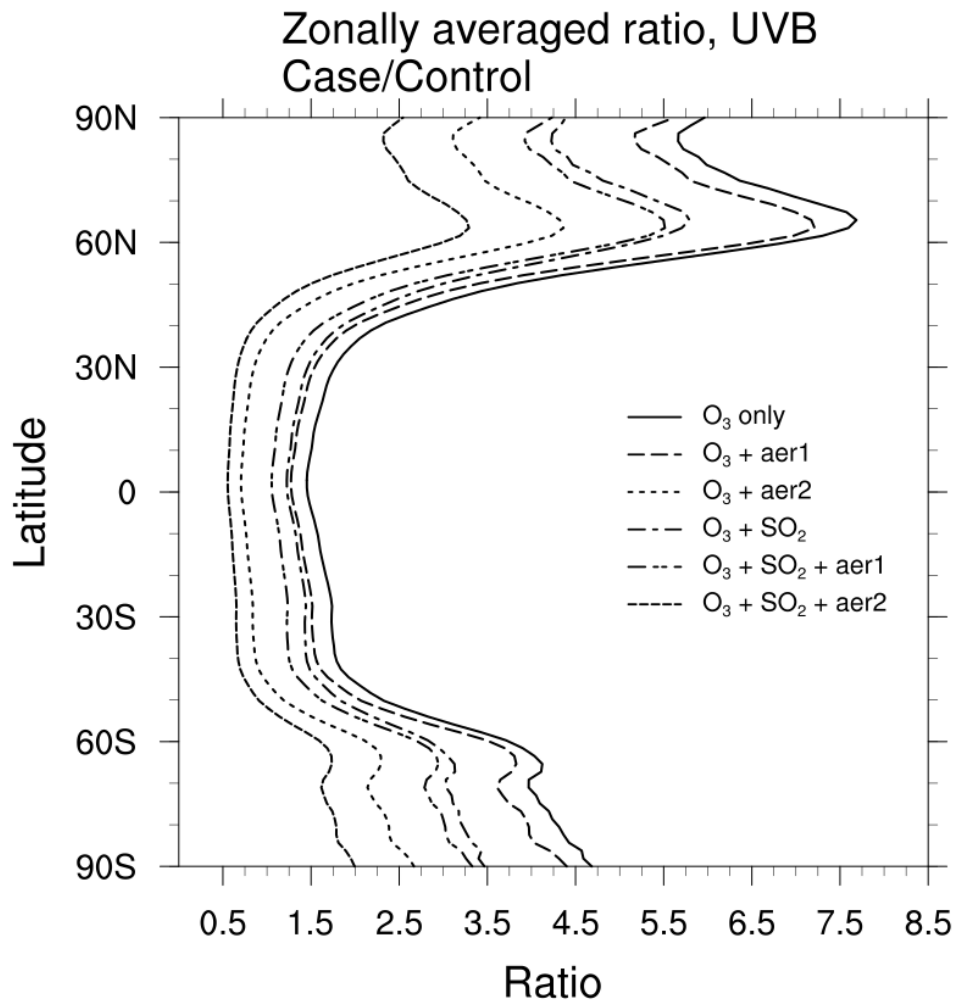


Figure 3 - Zonally averaged ratio of UVB irradiance for each of the volcanic cases (see Table 1) versus control.

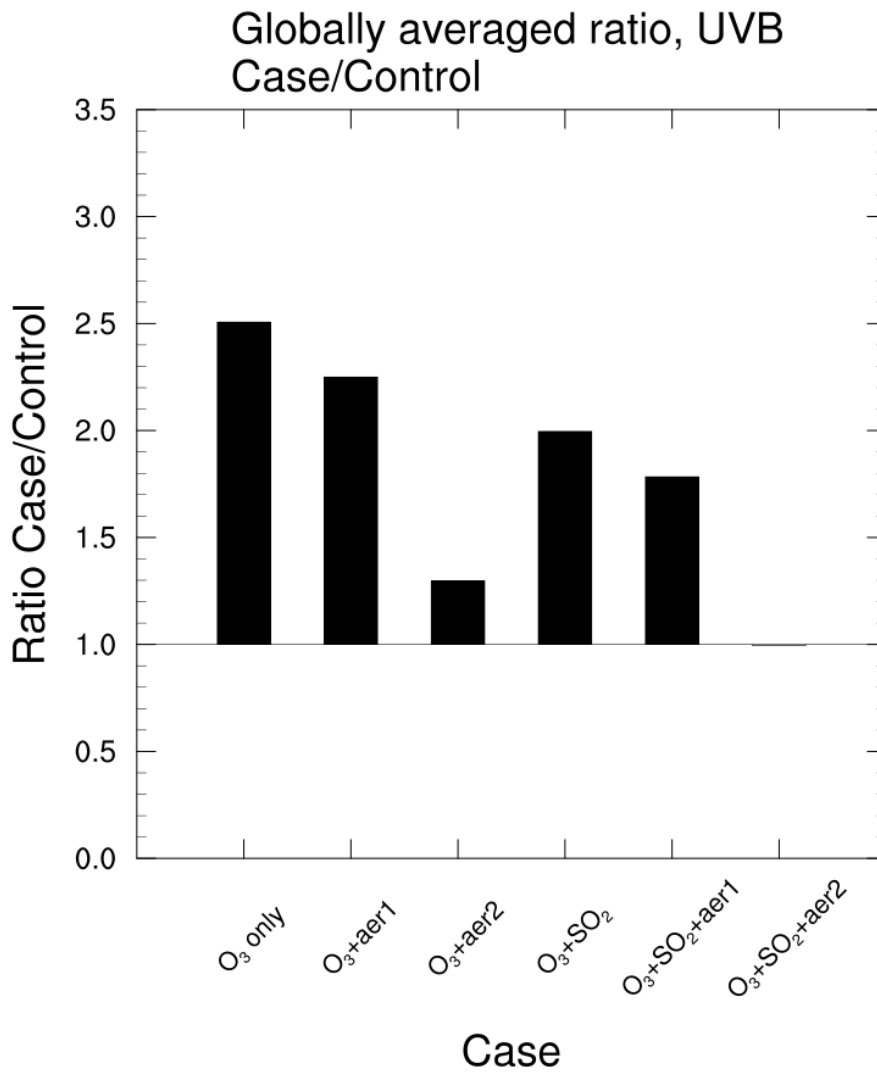


Figure 4 – Globally averaged ratio of UVB irradiance for each of the volcanic cases (see Table 1) versus control.

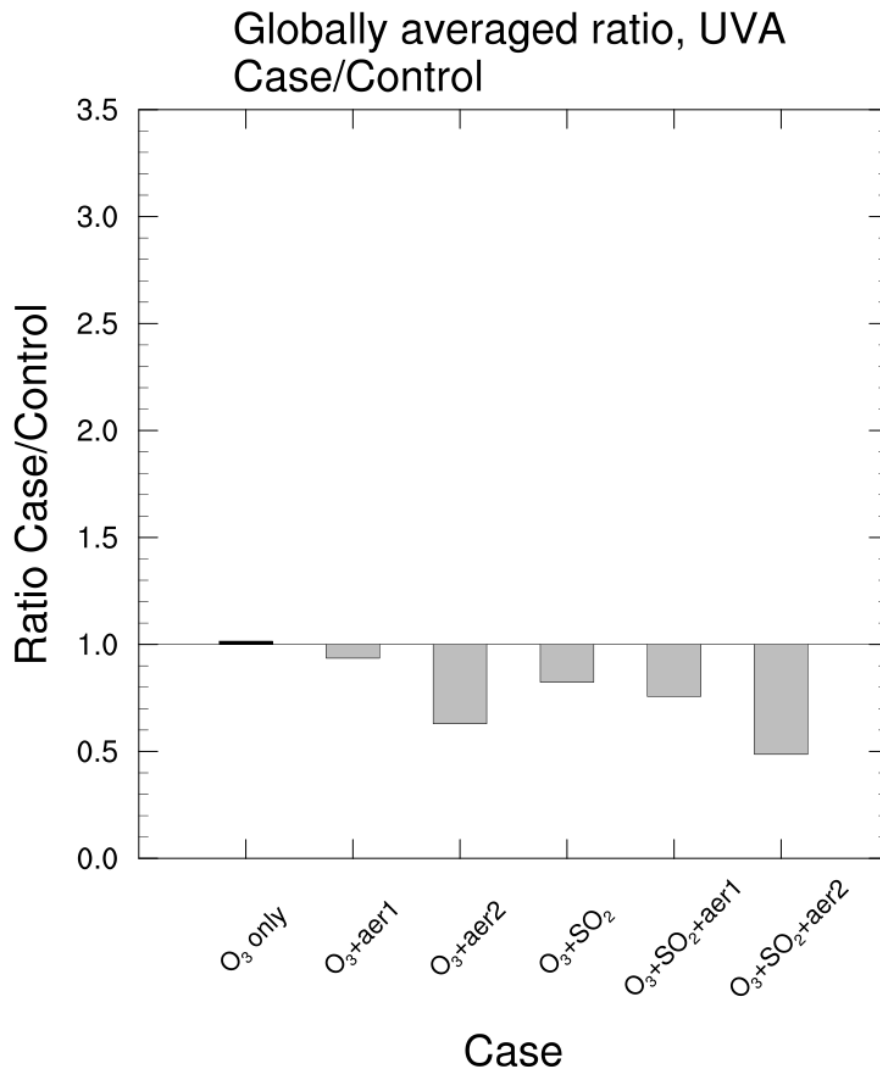


Figure 5 – Globally averaged ratio of UVA irradiance for each of the volcanic cases (see Table 1) versus control.

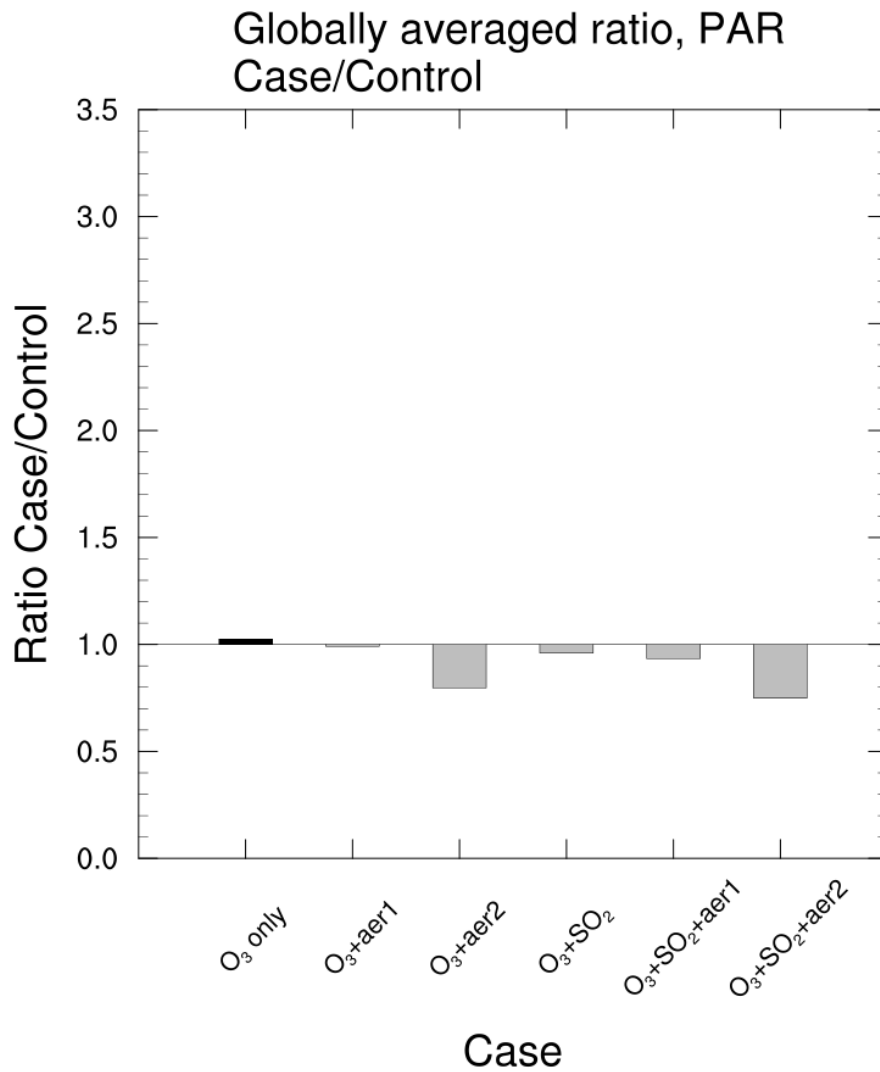


Figure 6 – Globally averaged ratio of PAR irradiance for each of the volcanic cases (see Table 1) versus control.

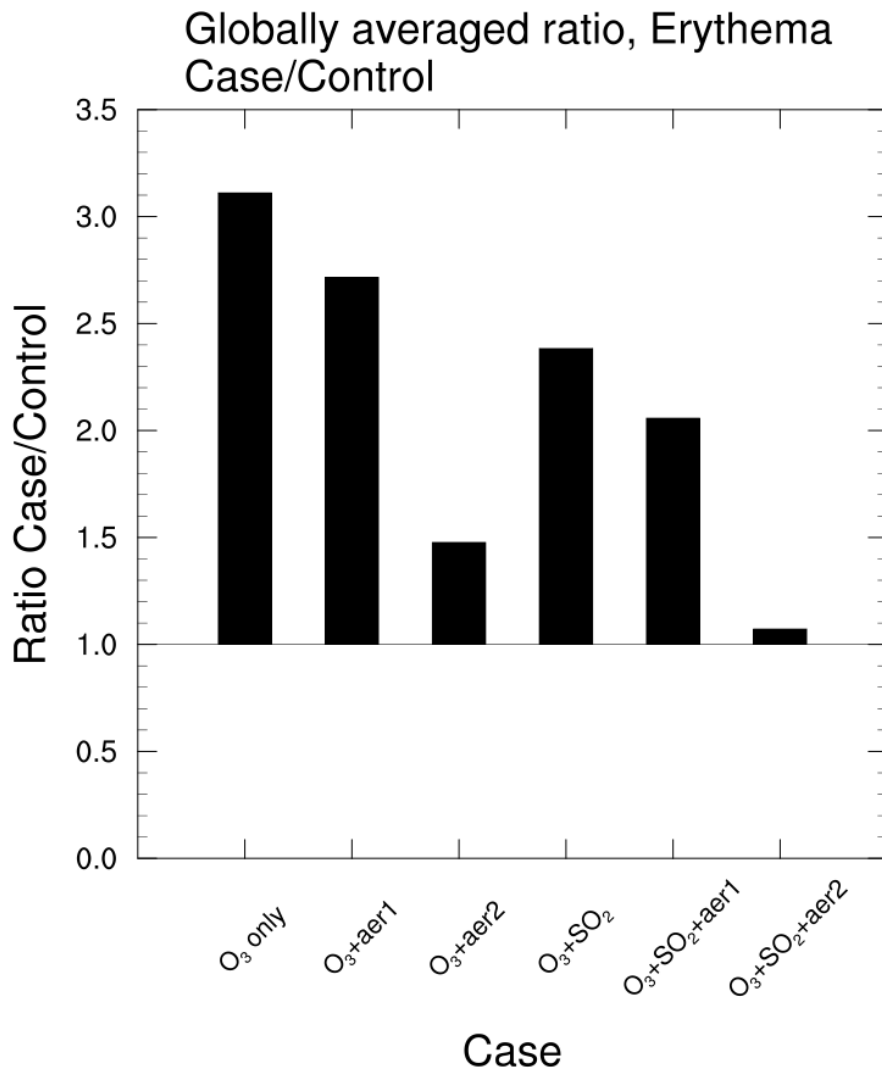


Figure 7 – Globally averaged ratio of Erythema-weighted irradiance for each of the volcanic cases (see Table 1) versus control.

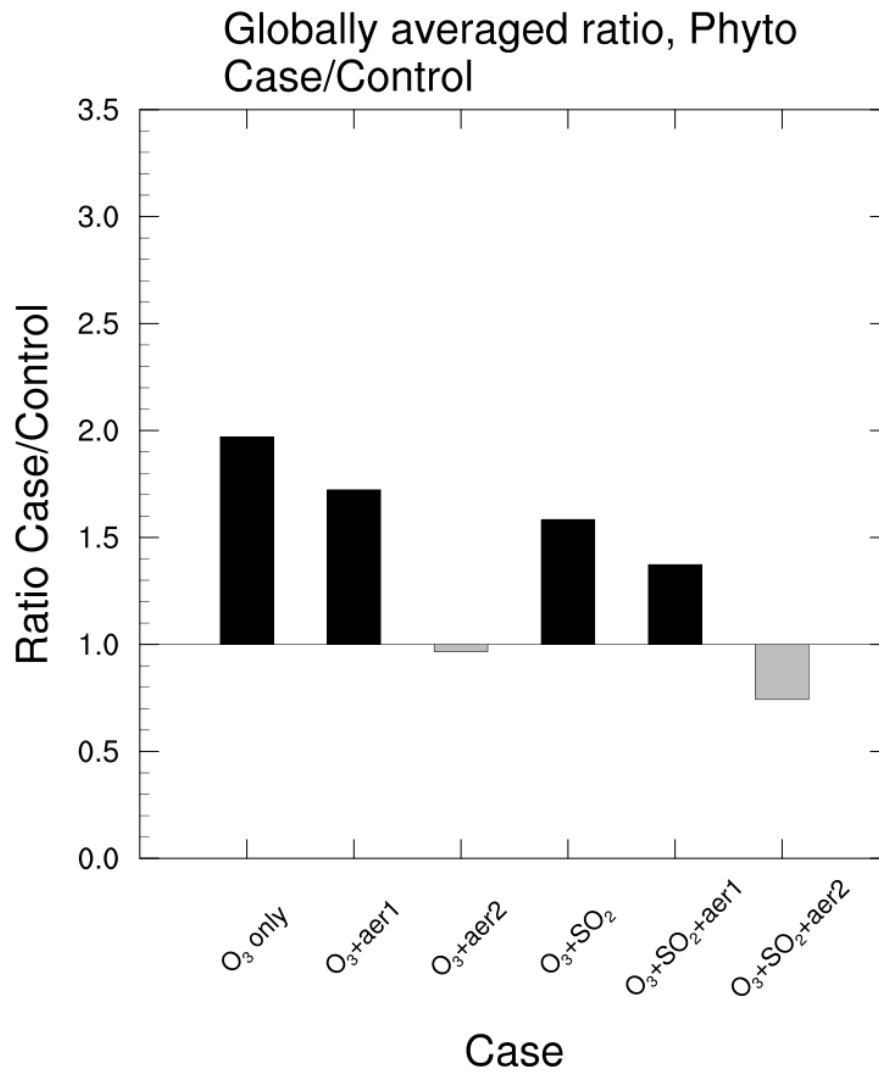


Figure 8 – Globally averaged ratio of phytoplankton photosynthesis inhibition-weighted irradiance (using a BWF for inhibition of carbon fixation in a natural Antarctic phytoplankton community²⁷) for each of the volcanic cases (see Table 1) versus control.

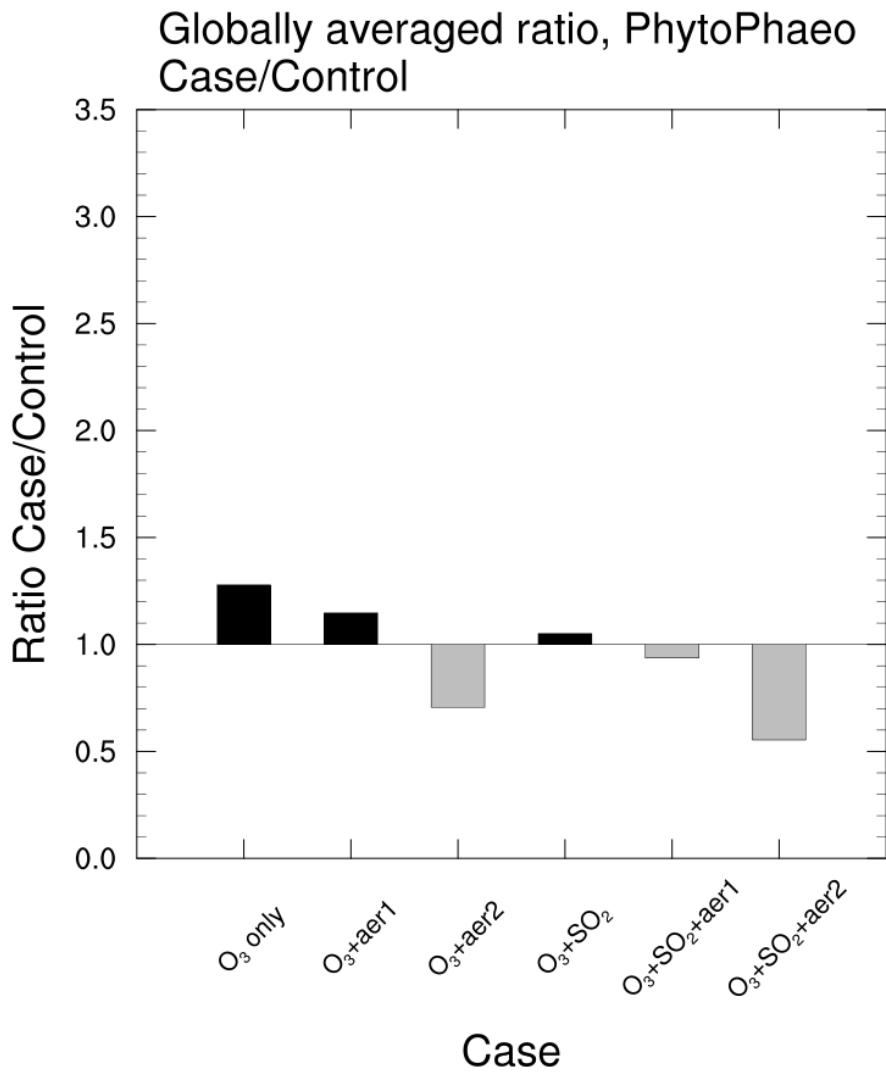


Figure 9 – Globally averaged ratio of phytoplankton photosynthesis inhibition-weighted irradiance (using a BWF for *Phaeo-dactylum*²⁸) for each of the volcanic cases (see Table 1) versus control.

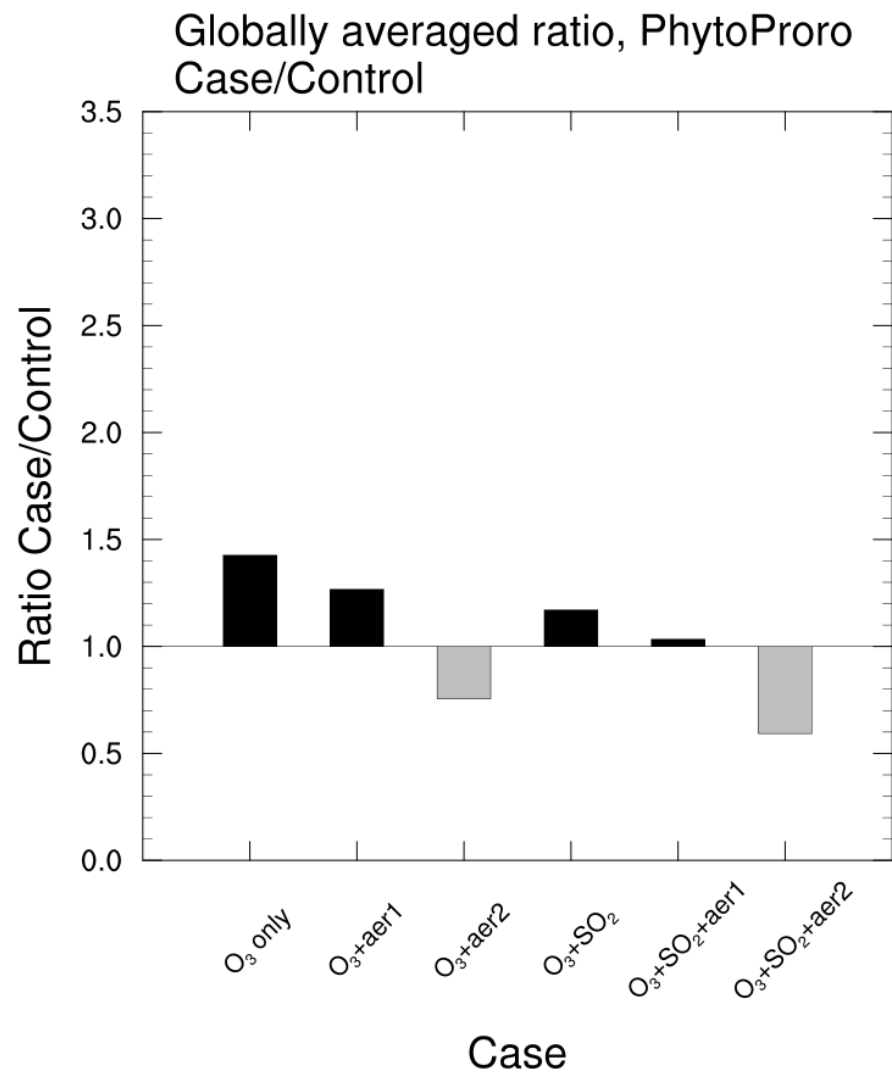


Figure 10 – Globally averaged ratio of phytoplankton photosynthesis inhibition-weighted irradiance (using a BWF for *Prorocentrum micans*²⁸) for each of the volcanic cases (see Table 1) versus control.

Globally averaged ratio, PlantDamageCaldwell71
Case/Control

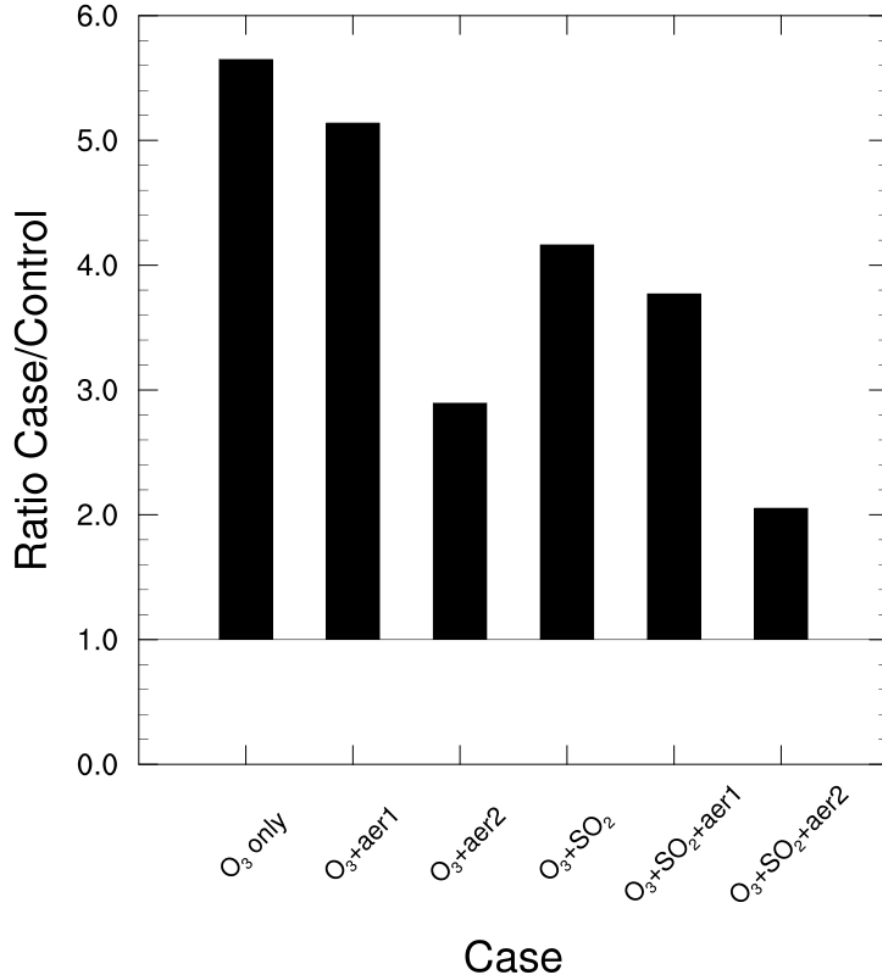


Figure 11 – Globally averaged ratio of plant damage-weighted³¹ irradiance for each of the volcanic cases (see Table 1) versus control. Note the vertical axis scale here is larger than in previous similar plots.

Globally averaged ratio, PlantDamageFlint_Caldwell03
Case/Control

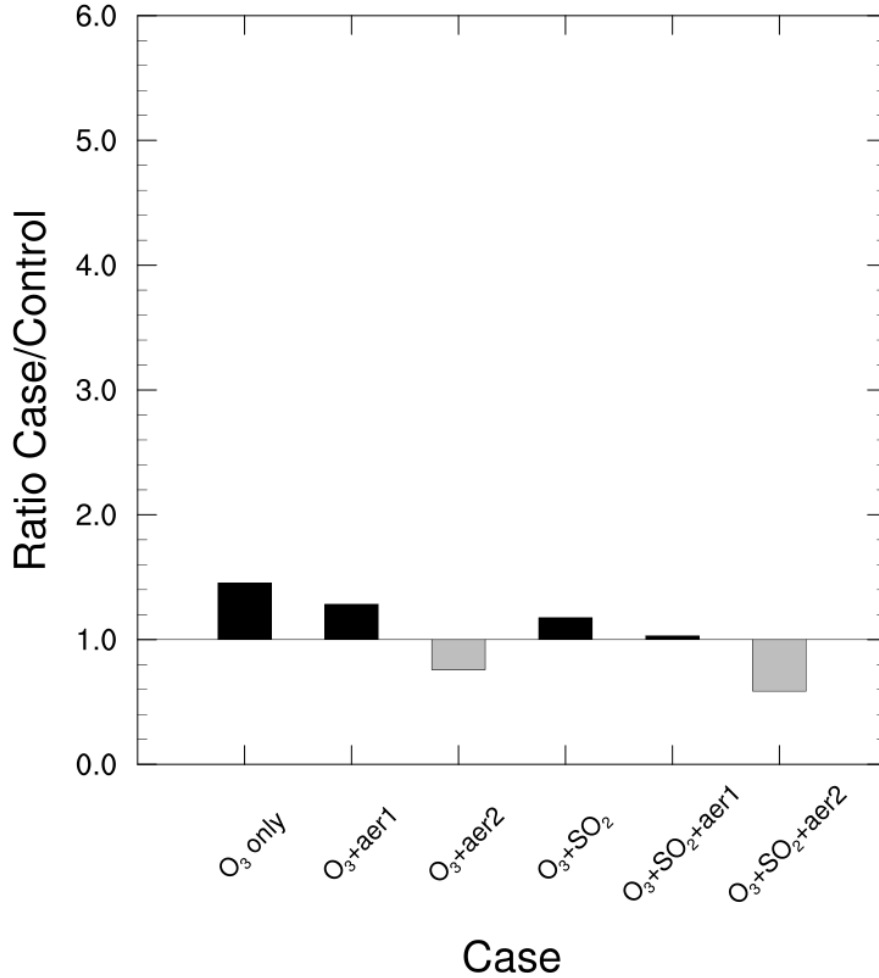


Figure 12 – Globally averaged ratio of plant damage-weighted³² irradiance for each of the volcanic cases (see Table 1) versus control. Note the vertical axis scale here is chosen for comparison with Figure 11.

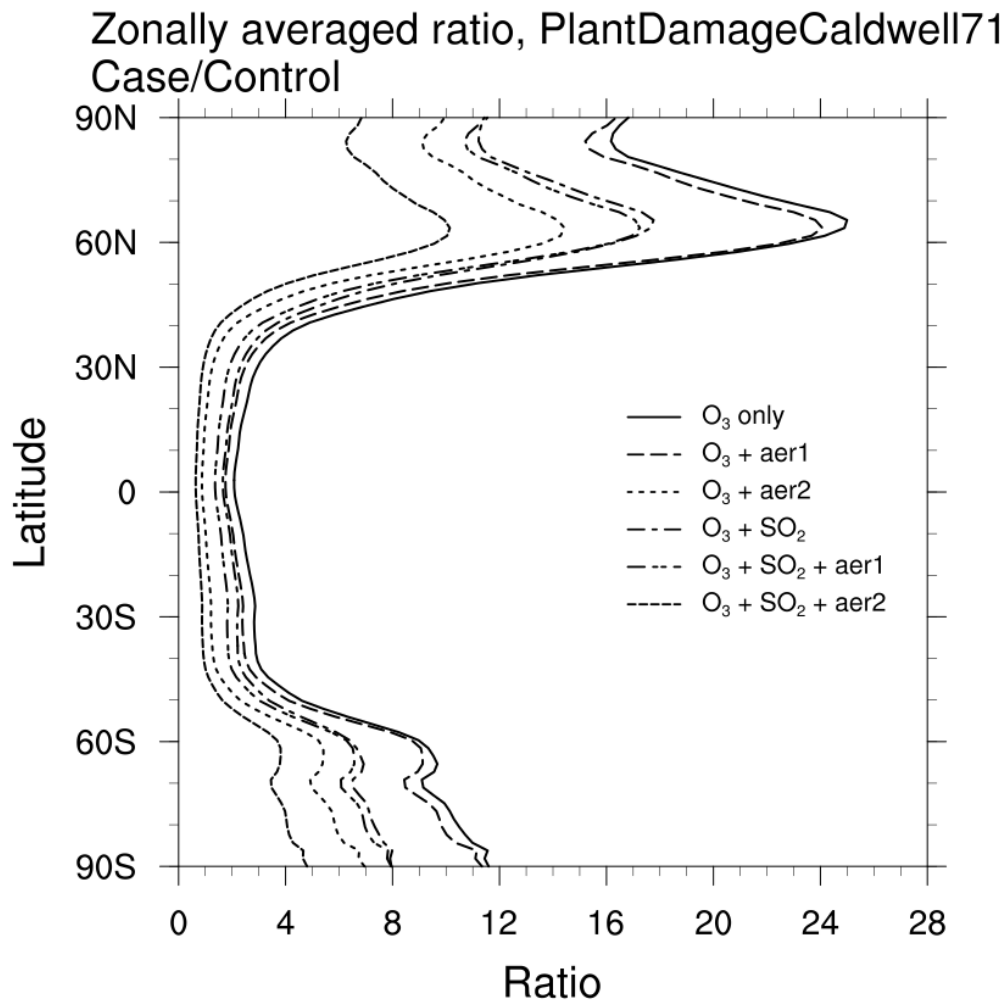


Figure 13 - Zonally averaged ratio of plant damage-weighted³¹ irradiance for each of the volcanic cases (see Table 1) versus control. Note the horizontal axis scale is larger than the comparable Figure 3.